Investigation of Local Heat Transfer in Compact Heat Exchangers by Holographic Interferometry

R. Fehle
J. Klas
F. Mayinger
Lehrstuhl A für Thermodynamik, Technische Universität München, München, Germany

■ Compact heat exchangers are key components for the development of future aircraft devices. An enhancement of the heat transfer results in a decrease in the heat exchanger size and thus in lower weight and lower investment costs. Exact knowledge of the temperature distribution in the boundary layer is necessary for a specific augmentation of heat transfer. Holographic interferometry was applied to visualize the temperature field. This optical measuring method offers the advantage of delivering information about the temperature distribution without disturbing the flow pattern. A digital image processing system was used for evaluation of the interferograms. The local Nusselt number was determined from the isotherms at the wall. Two types of geometries for compact plate heat exchangers were investigated using air as test fluid: plain fin arrangements of plate-fin heat exchangers and circular segment shaped turbulence promoters in plate heat exchangers. The test section was heated by hot water to obtain a constant wall temperature as a thermal boundary condition. During the experiments Re was varied between 500 and 3000, a range where low pressure losses occurred. Investigations of the plate-fin arrangements show that the Nusselt number for the geometry with 1-mm radii is about 15% higher than that for the duct with radii of 5 mm. In the case of the circular segment shaped turbulence promoters, a staggered, a nonstaggered, and an inclined arrangement were investigated. The overall Nusselt number shows that the nonstaggered ribs lead to the best heat transfer. To compare the results with the heat transfer in a flat duct, the Nusselt number distribution between parallel plates was calculated by equations taken from the literature. The present results show that an enhancement of heat transfer of 100% for low Reynolds numbers and approximately 300% for Re = 2500 can be achieved.

Keywords: *holographic interferometry, plate-fin heat exchangers, plain fin arrangement, turbulence promoters, local Nusselt number distributions, volume goodness factor*

INTRODUCTION

An enhancement of the heat transfer rate results in a decrease in the heat exchanger size. Generally the heat transfer rate in a heat exchanger can be calculated as

$$\dot{Q} = \Delta T_m U \beta V. \quad (1)$$

Therefore, improvements of heat transfer can be achieved by increasing the volume V or area density β of the heat exchanger, the logarithmic mean temperature difference ΔT_m, or the overall conductance U, including the heat transfer coefficients and the conductivity of the wall. The convective heat transfer coefficient of gases usually is one or two orders of magnitude lower than that of liquids. For this reason a large heat transfer area is necessary for realizing a high heat transfer rate, especially if one or more fluids are gaseous. This means that the surface must be compact. A heat exchanger is considered compact if it incorporates at least one compact surface [1]. Shah [2] specifies that a surface is compact if the area density is greater than 700 m^2/m^3. In practice this value is often exceeded. For a specific improvement of heat exchanger surfaces, exact knowledge of the temperature distribution, especially in the boundary layer, is useful. Because of the thin boundary layer it is impossible to apply a direct mechanical measuring gauge. For this reason, holographic interferometry, a combination of holography and interferometry, was chosen to visualize the temperature field

Address correspondence to R. Fehle, Lehrstuhl A für Thermodynamik, Technische Universität München, Arcisstrasse 21, D-80290 München, Germany.

Experimental Thermal and Fluid Science 1995; 10:181–191

655 Avenue of the Americas, New York, NY 10010

0894-1777/95/$9.50
SSDI 0894-1777(94)00088-P

continuously without disturbing the flow pattern. An explanation of this well-known measuring technique, described by Hauf and Grigull [3], Chen and Mayinger [4], and Mayinger and Panknin [5], is omitted from this paper. But for better understanding of the interferogram it should be mentioned that the interference lines of them are approximately identical to the isotherms of the investigated duct flows. From the distance between isotherms, the heat flux and therefor the local Nusselt number distribution can be calculated. With this knowledge the efficiency of heat transfer can be improved specifically.

The low Reynolds number range between 500 and 3000 is quite interesting for the aerospace industry. Due to the low density of air at great altitudes, low Reynolds numbers occur quite often in aircraft applications.

THE EXPERIMENTAL SETUP

The experimental setup for investigating the plain fin arrangements is shown in Fig. 1. The test section has a sandwich construction, with the removable upper part enabling the employment of different test matrices of variable height and size or of differently arranged but identically shaped turbulence promoters. The thermally insulated inlet section leads to a hydrodynamically developed airflow with a thermally developing flow regime in the ducts. The test section itself is heated by six water-supplied heating plates. The temperature of each plate is measured by thermocouples in order to obtain a uniform wall temperature of the test matrix surface. In the case of the plain fin arrangement, the laser beam passes through the test chamber in the same direction as the fluid flow and leaves it at the exit through an ordinary sheet of glass covering the outlet of the test section. In the other case the laser bean penetrates the test section along the circular segment shaped turbulence promoters perpendicular to the flow direction so that the side walls have to be kept transparent. Mass flow rates and thus Reynolds numbers in the test matrix are determined by orifices with an accuracy of 3%. Air temperatures at the entrance and exit of the test matrix are measured by seven thermocouples, allowing a calculation of the logarithmic mean temperature difference. Due to the measurement uncertainties an accuracy of the global heat balance (see next Section) of less than 10% is reached. Airflow is produced by a suction pump equipped with a flow-regulating throttle.

A digital image processing system is employed to evaluate the interferograms. The interference patterns are filmed with a CCD camera and changed into digital images of 768–512 points by a digitizer board fixed to a PC-AT. An interactive control program was written for this system. Several possibilities exist for improving the quality of the interferograms, including digital filters and contrast-enhancing and noise-reducing procedures. Within this program the distribution of gray values along lines normal to the surface of the test matrix can be scanned. Local maximum and minimum gray values along these lines are obtained automatically in order to determine the distance between the interference lines. From this the temperature field and the local heat transfer coefficients can be determined.

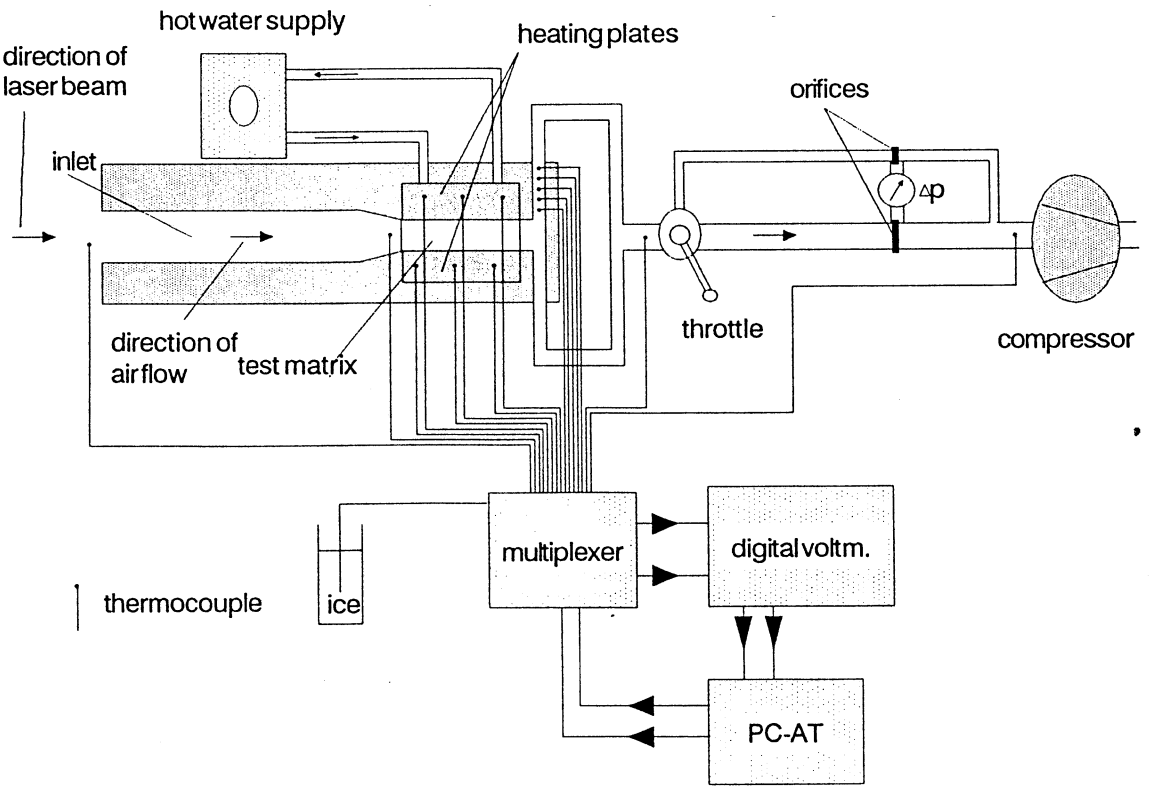

Figure 1. Experimental setup.

Table 1. Dimensions (mm) of Plain Fin Arrangements

	Matrix 1	*Matrix 2*	*Matrix 3*
Height of fins e	10	10	10
Width of duct b	10	10	10
Length l_r	300	300	300
Fin thickness t_f	2	2	2
Radius r	1	3	5

HEAT TRANSFER IN PLAIN FIN ARRANGEMENTS

During the first phase of our experiments the heat transfer in plain fin arrangements presented in Fig. 2 was investigated. Three test matrices with corner radii r of 1, 3, and 5 mm were manufactured. The ducts were milled out of 12-mm-thick sheets of aluminum with a fin thickness of 2 mm. The exact dimensions are summarized in Table 1. The hydraulic diameter d_{hyd} of the ducts is calculated from

$$d_{hyd} = 4A_c l/A, \tag{2}$$

considering the flow cross-sectional area A_c, the duct length l, and the total heat transfer area A.

Two typical interference patterns are presented in Fig. 3 for different corner radii, showing the temperature distribution averaged over the whole length of the test section. Due to this length, the temperature difference between two neighboring isotherms is approximately 2.3 K. The local Nusselt number Nu_α is determined as

$$\mathrm{Nu}_\alpha = h_\alpha d_{hyd}/k, \tag{3}$$

where h_α is the local heat transfer coefficient and k the thermal conductivity of air, with

$$h_\alpha = \dot{q}_\alpha/\Delta T_m, \tag{4}$$

where $\dot{q}_\alpha$ is the local heat flux density expressed as

$$\dot{q}_\alpha = k\left(\frac{dT}{dy}\right)_w \tag{5}$$

with $(dT/dy)_w$ as the temperature gradient perpendicular to the surface at the wall. Figures 4–6 show the local Nusselt number distribution at Reynolds numbers of 500, 1500, and 2500, respectively. Comparing these figures one can easily recognize that the local heat transfer is proportional to the fringe density at the corresponding wall. Due to digitizing effects and light deflections, an uncertainty in the measuring technique of less than 10% was achieved.

For low Reynolds numbers, typical laminar flow patterns are established, resulting in maximum heat transfer in the middle between two adjacent corners. On the other hand, the heat flux decreases at the corners. It seems that the heat flux vanishes at the convex corners because the flow is stagnant in this area.

Similar results could be found in the literature. Marco and Han [6] present an analytical study of a hydrodynamic fully developed flow in a square channel resulting in a distribution of the local Nusselt number comparable with ours. The ratio of the local Nusselt number to the average along one side is shown in Fig. 7. Near the corners the convective energy transport goes down toward zero due to a strong decrease in the flow velocity. On the other hand, the flow velocity increases along the wall, and therefore a maximum of the ratio of Nusselt numbers appears in the middle of each side. This curve was confirmed by Luo and Cai [7] and Kato and Maruyama [8].

In the case of turbulent flow in a rectangular channel, the velocity profile is influenced by secondary flow near the corners [9, 10]. In consequence of this flow pattern, the maximum of the local Nusselt number moves toward the corners in comparison with the laminar flow. Now a local minimum appears in the middle of the wall. Figure 7 also shows the experimental results of Brundrett and Burroughs [11]. At a Reynolds number of 2500 the measurements with the plain fin arrangements show results that are in good agreement with the cited literature for turbulent flow. The described typical Nusselt number distribution can be observed near the convex radii where local maxima of the heat flux occur in the direct neighborhood of the corners and a local minimum in the middle of this side. In contrast with the laminar flow, the heat flux decreases only in the immediate vicinity of the convex corners.

To compare the heat transfer behavior of the different investigated arrangements and to verify the interferometric data, the local Nusselt numbers are integrated over the whole heat transfer surface. On the other hand, average Nusselt numbers

$$\mathrm{Nu} = hd_{hyd}/k, \tag{6}$$

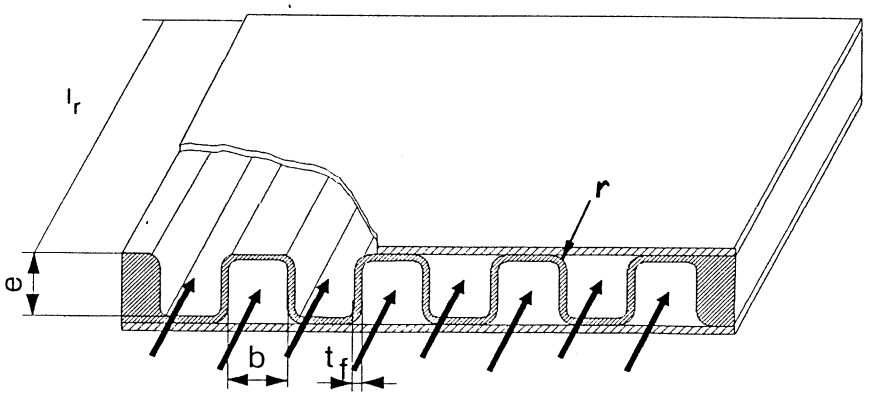

Figure 2. Plain fin arrangement in compact plate heat exchangers.

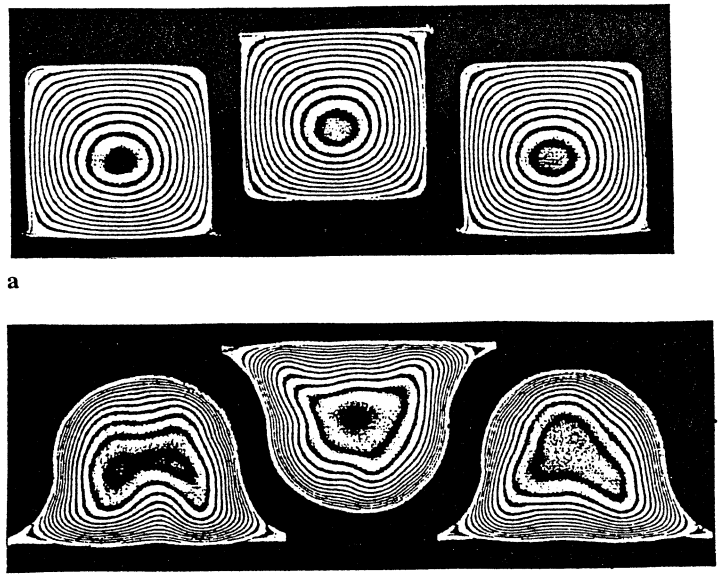

a

b

Figure 3. Interferograms for plain fin arrangements: (*a*) $r = 1$ mm, Re = 500, (*b*) $r = 5$ mm, Re = 2500.

with h as the average heat transfer coefficient, can also be obtained from the energy balance

$$\dot{m} c_p [T_{out} - T_{in}] = hA \, \Delta T_m, \tag{7}$$

where $\dot{m}$ is the air mass flow rate, c_p the specific heat capacity at constant pressure, and T_{in} and T_{out} the average temperatures of the fluid at the inlet and outlet of the channels. Figure 8 shows the average Nusselt numbers calculated from the interferograms and from the energy balance as a function of Reynolds number. Comparing the Nusselt numbers, the high accuracy of the measuring technique is demonstrated by the small difference, less than 7%, between the overall heat balance and the interferometric measurements.

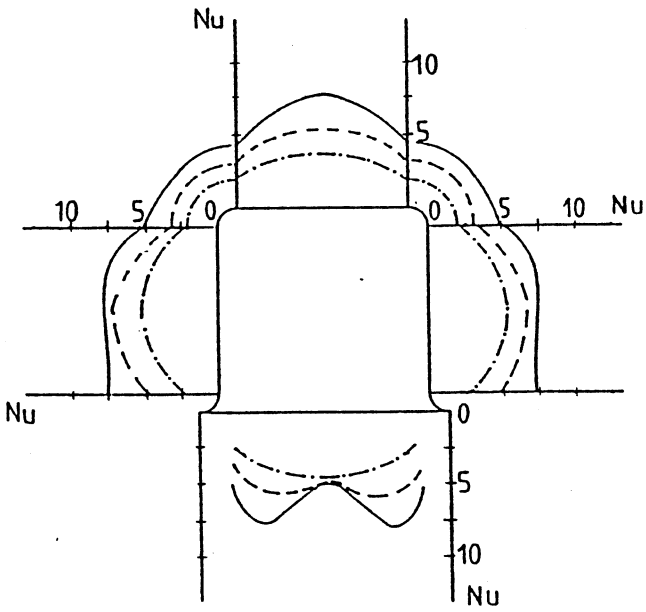

Figure 4. Local distribution of Nusselt number for square ducts with corner radii of 1 mm. (——) Re = 2500, (- - -) Re = 1500, (-·-) Re = 500.

The duct with a corner radius of 1 mm leads to the maximum Nusselt numbers, whereas the lowest Nusselt numbers were measured for the test matrix with radii of 5 mm. The Nusselt number for the geometry with 1-mm radius is about 15% higher than that for the duct with radius of 5 mm.

Comparing different heat exchangers, the heat transfer rate and the pressure drop are the decisive parameters. The aim of heat exchanger design is to get a high heat flux combined with a pressure drop as low as possible. One way to compare different geometries uses the volume goodness factor. London and Ferguson [12] propose the heat transfer coefficient h as a function of the pumping power P per heat transfer area A, determined by

$$E = \frac{P}{A} = \frac{1}{8 d_{hyd}^3} \xi \, \mathrm{Re}^3 \, \rho \nu^3, \tag{8}$$

where ξ is the pressure drop coefficient and ν the kinetic viscosity. Equation (8) is suitable for a comparison of heat exchangers with the same hydraulic diameter. In the case of different hydraulic diameters, Kays and London [13] recommend multiplying the heat transfer coefficient h by the fin efficiency η_R and the area density β and showing it as a function of the product $E\beta$. The volume goodness factor is

$$\frac{\dot{Q}/V}{P/V} = \frac{\eta_R h \, \Delta T_m \, \beta}{\beta} \sim \frac{h \beta \eta_R}{E\beta}, \tag{9}$$

and the higher it is, the bigger is the heat flux per unit volume to be transferred, maintaining the same temperature difference and the same pumping power per unit volume. Figure 9 shows the volume goodness factor of the three investigated arrangements with the fin efficiency set equal to 1. The ducts with bent radii of 5 mm transfer the highest heat flux per unit volume for the same pumping power per unit volume. This result seems to contrast with

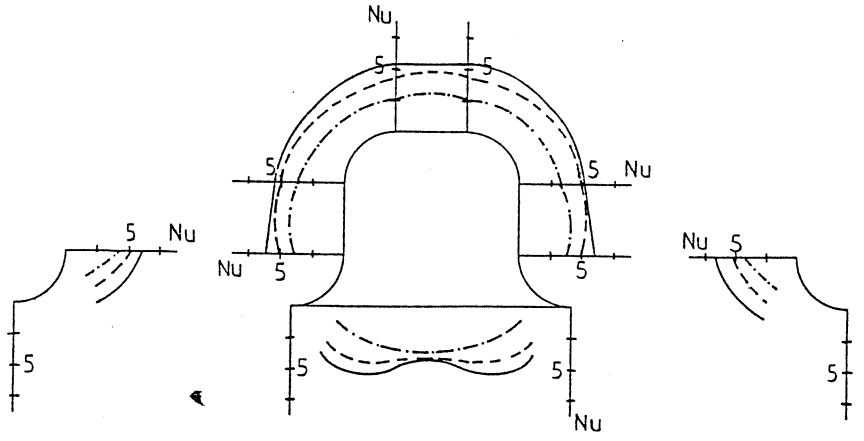

Figure 5. Local distribution of Nusselt number for square ducts with corner radii of 3 mm. (——) Re = 2500, (- - -) Re = 1500, (–·–) Re = 500.

the presented Nusselt number distribution. This is because this design delivers the biggest heat transfer area or area density resulting in the highest heat transfer rate per heat exchanger volume connected with the lowest pressure drop coefficient ξ.

CIRCULAR SEGMENT SHAPED TURBULENCE PROMOTERS

Turbulence promoters often lead to a considerable enhancement of the heat transfer. Rectangular obstacles cause relatively high pressure losses with flow separations at the rib. To avoid sharp edges, ribs can be circular. To study the influence of circular segment shaped ribs, two test matrices were manufactured and connected to form the rectangular duct illustrated in Fig. 10. The test duct consists of two wide, ribbed sides and two small plain spacers made of glass. Due to the aspect ratio of the test section (duct height $d = 1$ cm, duct width $b = 15$ cm), an almost two-dimensional flow pattern can be assumed. By rotating one plate, we could investigate both staggered and nonstaggered fin arrangements. In addition a section was tested with ribs inclined at an angle of 20° to the flow, with the ribs oriented opposite each other on the two walls, leading to a crossed-rib arrangement. Rib dimensions and rib pitch were held constant during the experiments.

For the parallel plates, the hydraulic diameter d_{hyd} is given by

$$d_{hyd} = 2d. \tag{10}$$

The characteristic data for this geometry are given in Table 2. Figure 11 shows interferograms for different arrangements taken at Re = 1500. At this condition the effect of the ribs as turbulence promoters is ascertained. Whereas the flow is laminar in the entrance region of the duct, it changes to turbulent between the third and fifth ribs, resulting in a highly increased Reynolds number. This effect can be observed in Fig. 12, where the temperature profiles are shown for the wakes of the first and fifth ribs. In Fig. 12*a*, the largest temperature drop occurs in the center of the duct, whereas the temperature gradient is noticeably high close to the wall for turbulent flow. For the latter, a relatively low temperature gradient was noticed in the duct middle. The inlet effect on the heat transfer is depicted for the staggered arrangement in Fig. 13. The heat transfer in the wake of the first rib is relatively low due to the laminar flow condition and increases by 150% in the wake of the five following ribs.

The local Nusselt number distribution at the fifth obstacle and in the following groove is illustrated in Figs. 14 and 15, which describe a fully developed flow. A comparison with the behavior at the downstream and upstream ribs confirms a fully developed flow with a heat transfer that is no longer dependent on rib number. The heat transfer along the obstacle is maximum for the nonstaggered ribs. The minimum flow cross section between the ribs compared to the other arrangements leads to high local velocities and therefore to increased convective heat fluxes. On the other hand, the heat transfer is relatively low for the staggered ribs. In the gap between the obsta-

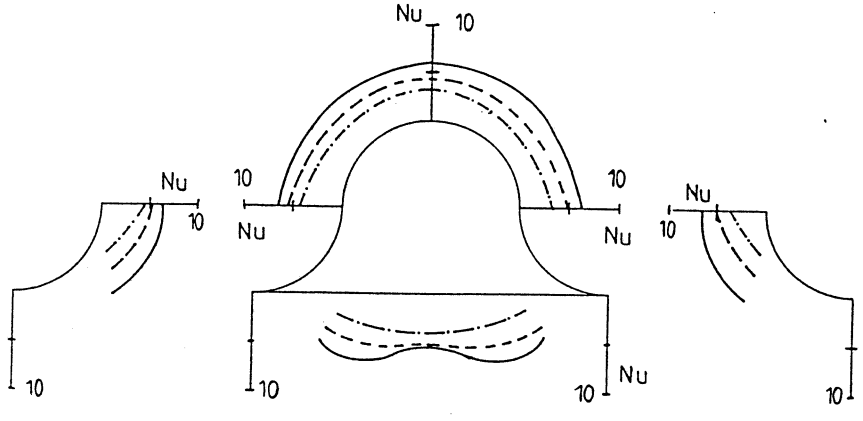

Figure 6. Local distribution of Nusselt number for square ducts with corner radii of 5 mm. (——) Re = 2500, (- - -) Re = 1500, (–·–) Re = 500.

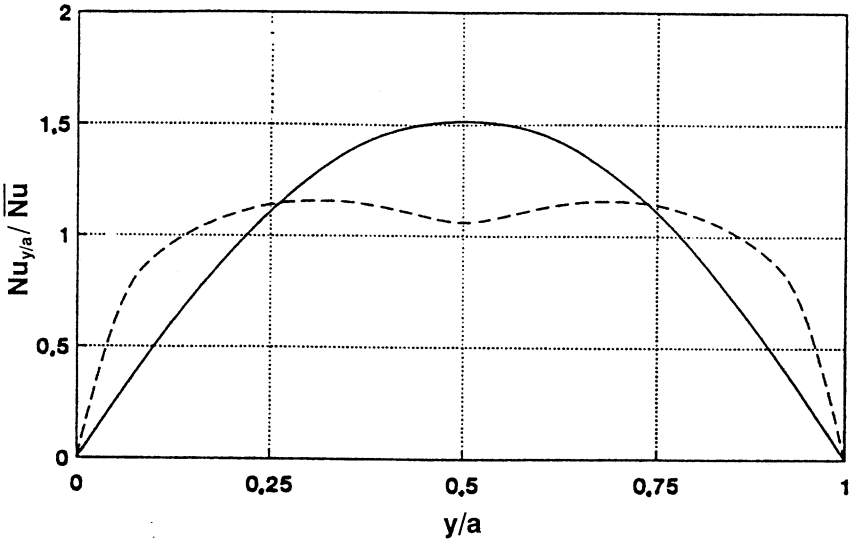

Figure 7. Local Nusselt number distribution for laminar and turbulent flow in a square channel. (——) Laminar [6]; (- - -) turbulent [11].

cles, the nonstaggered ribs show only very small heat transfer coefficients for laminar flow. The main mass flow was found in the center of the duct, with a widely decreasing convective part of the heat transfer in the wake of the ribs. The Nusselt number reaches only about 15% of the maximum value immediately after the rib at the obstacle itself and increases slightly to approximately 25% at the following rib. In this region both the other arrangements show better heat transfer rates, with maximum heat transfer at approximately half the distance between ribs.

In Fig. 15 the corresponding distribution for turbulent flow (Re = 2500) is illustrated. The Nusselt number shows almost the same behavior along the rib as for laminar flow conditions, but with increased values. Due to turbulence effects the heat transfer between ribs is enhanced to the same level as at the rib itself. For all investigated geometrics a maximum of heat transfer arises between one-half and two-thirds of the distance downstream from the rib. It is obvious that the heat transfer at nonstaggered ribs is about 25% higher than for the two other geometries and decreases more than for the other arrangements subsequent to each rib.

The overall Nusselt number was measured by energy balance methods also in order to confirm the results of the interferometric measurements. In Fig. 16 it can be seen that the nonstaggered ribs lead to the best heat transfer. The staggered and inclined arrangements show basically similar behavior, with slight advantages in heat transfer for the inclined ribs. The interferometric measurements correspond with the caloric results for Reynolds numbers of 500 and 1500 within a range of 5%. For a Reynolds number of 2500 a difference of 15% occurs, probably due to the thin boundary layer at the obstacles. In Fig. 16, the heat transfer in a flat duct, that is, between

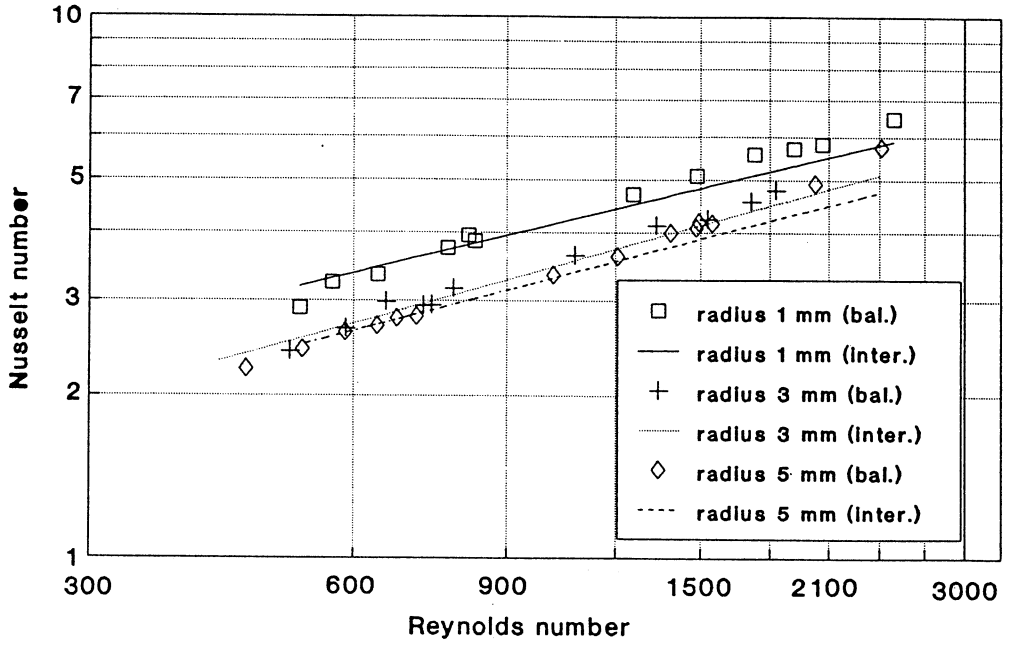

Figure 8. Nusselt number as a function of Reynolds number for plain fin arrangements.

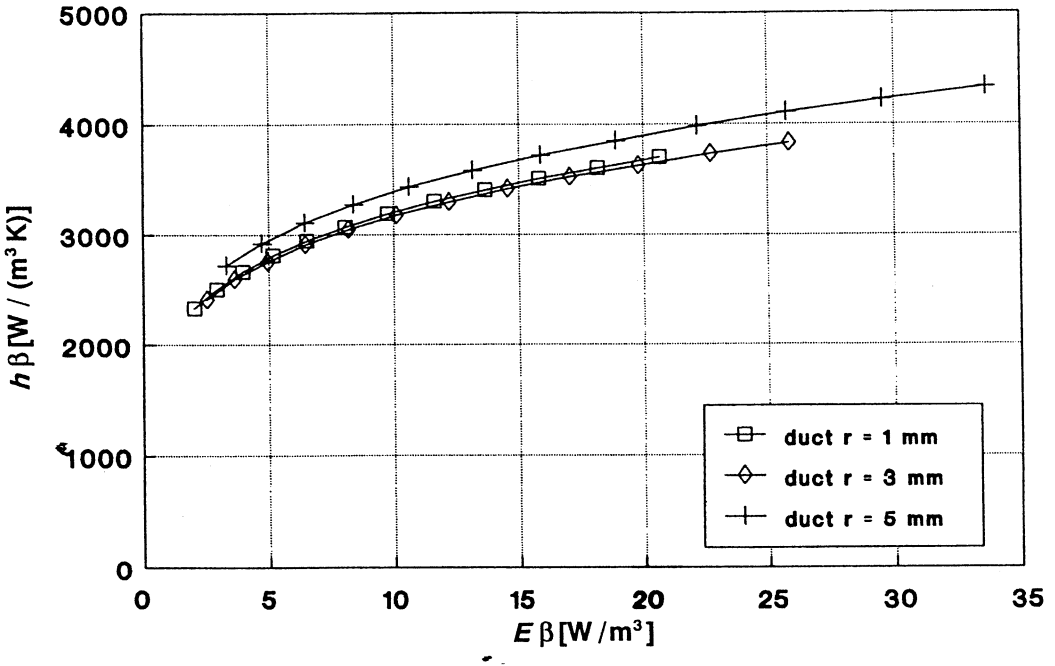

Figure 9. Volume goodness factor for plain fin arrangements with different corner radii ($\eta_R = 1$).

parallel plates, is shown for comparison; it was calculated by equations given by Kays and London [13]. The present results show that a 100% enhancement of heat transfer for low Reynolds numbers and approximately 300% for Re 2500 can be achieved.

The determined volume goodness factor for the various arrangements is shown in Fig. 17. The staggered ribs, in spite of having the lowest Nusselt numbers, give the highest volume goodness factor because they also give the lowest pressure drop. This arrangement transfers the greatest heat flux for a given pumping power. Despite showing the best heat transfer behavior the nonstaggered design proves to be the most unfavorable because of its high pressure losses. Nevertheless, each of the investigated arrangements shows clearly better behavior than parallel plates.

PRACTICAL USEFULNESS / SIGNIFICANCE

By enhancing the efficiency of heat exchangers, the overall efficiency of a heat exchanger system can be increased. An important aspect is the improvement of heat transfer.

The local heat transfer behavior of various compact plate heat exchangers was investigated. The arrangements were compared with respect to the volume goodness factor, which takes not only the heat transfer into account but also the pressure drop. In the case of the plain fin arrangement, small corner radii turned out to give the

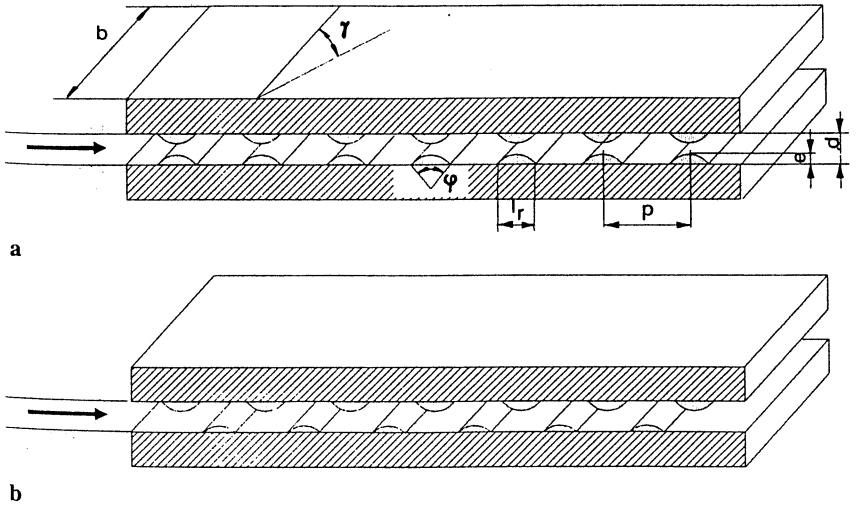

Figure 10. Nonstaggered (*a*) and staggered (*b*) arrangements of investigated turbulence promoters.

Table 2. Dimensions of Plain Fin Arrangements

	Matrix a	*Matrix b*
Height of duct d (mm)	10	10
Width of duct b (mm)	150	1500
Height of ribs e (mm)	3	3
Length of ribs l_r (mm)	10	10
Circular segment angle φ	120°	120°
Rib spacing p (mm)	30	30
Angle of attack γ	0°	20°
Arrangement	Staggered, nonstaggered	Inclined

best heat transfer behavior, but large corner radii gave the highest volume goodness factor. In addition, investigations of plate-fin heat exchangers with circular segment shaped ribs as turbulence promoters showed that the arrangement with the best heat transfer behavior (nonstaggered) is not the same as the arrangement with the best volume goodness factor (staggered).

CONCLUSIONS

The heat transfer behavior of compact plate-fin exchangers was investigated. As a measuring method, holographic interferometry was applied, enabling a noninvasive and inertialess visualization of the whole temperature field and therefore the determination of local Nusselt numbers.

First the heat transfer in plain fin arrangements was investigated to determine the influence of corner radii of the bent metal sheets of the ribs. The Reynolds number range extended from 500 to 3000, and a transition from laminar to turbulent flow was observed at about Re = 2000. The ducts with the smallest radii resulted in the highest Nusselt number for a given Reynolds number, Nu exceeding that of ducts with the largest radii by about 15%. However, a comparison of the investigated geometries in terms of the volume goodness factor showed that the ducts with the greatest radii were most advantageous.

Second, the influence of circular segment shaped turbulence promoters in staggered, nonstaggered, and inclined arrangements was examined. The determination of average Nusselt numbers showed that the nonstaggered geometry delivers the highest heat transfer rates. The best volume goodness factor was achieved with the staggered arrangement.

NOMENCLATURE

- a channel height, dimensionless
- A total heat transfer area, m^2
- A_c flow cross-sectional area, m^2
- b width of duct, m
- c_p specific heat capacity at constant pressure, J/(kg K)
- d height of duct, m

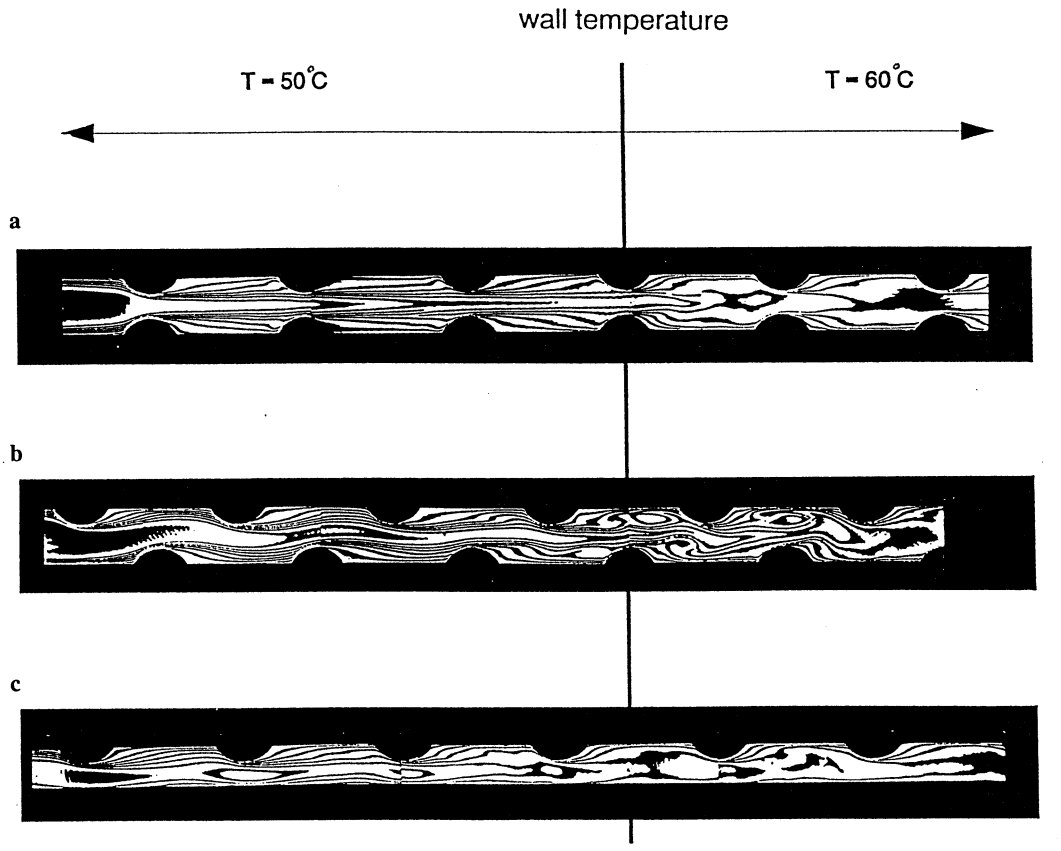

Figure 11. Interferograms of circular segment shaped ribs (Re = 1500). (*a*) nonstaggered, (*b*) staggered, (*c*) aligned.

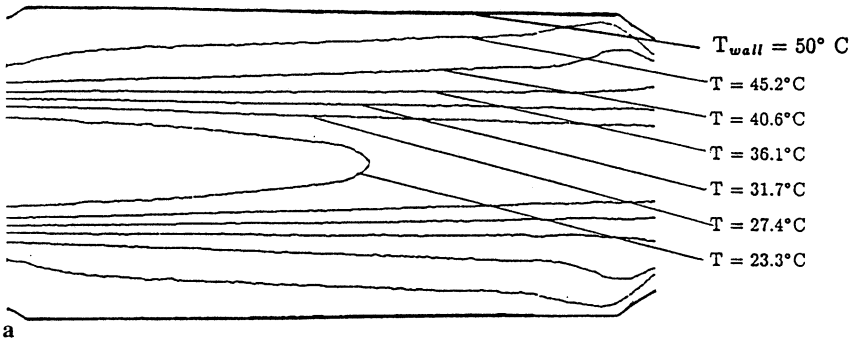

a

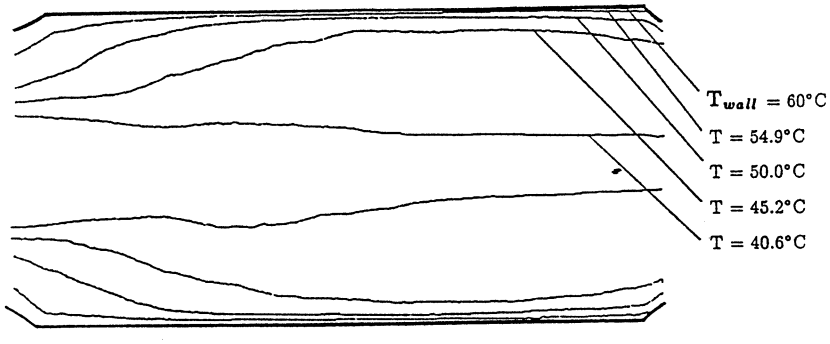

b

Figure 12. Temperature profiles in the wake of the first (*a*) and the fifth (*b*) rib (nonstaggered arrangement).

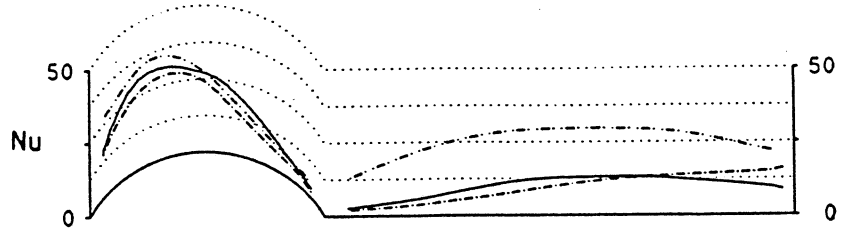

Figure 13. Entrance effects and heat transfer enhancement for Re = 1500 (staggered arrangement). Measurements taken in wake of (-···-) fifth rib, (-··-) third rib, (——) first rib.

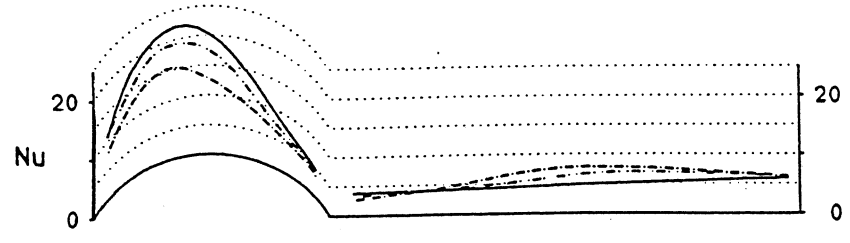

Figure 14. Local Nusselt number distribution for laminar flow (Re = 500) after the fifth rib. Arrangement of ribs: (-···-) inclined, (-··-) staggered, (——) nonstaggered.

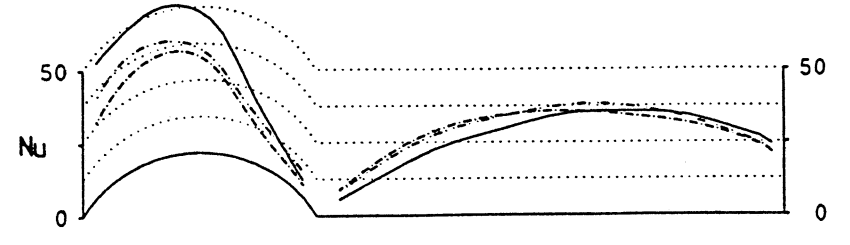

Figure 15. Local Nusselt number distribution for a turbulent flow (Re = 2500) after the fifth rib. Arrangement of ribs: (-···-) inclined, (-··-) staggered, (——) nonstaggered.

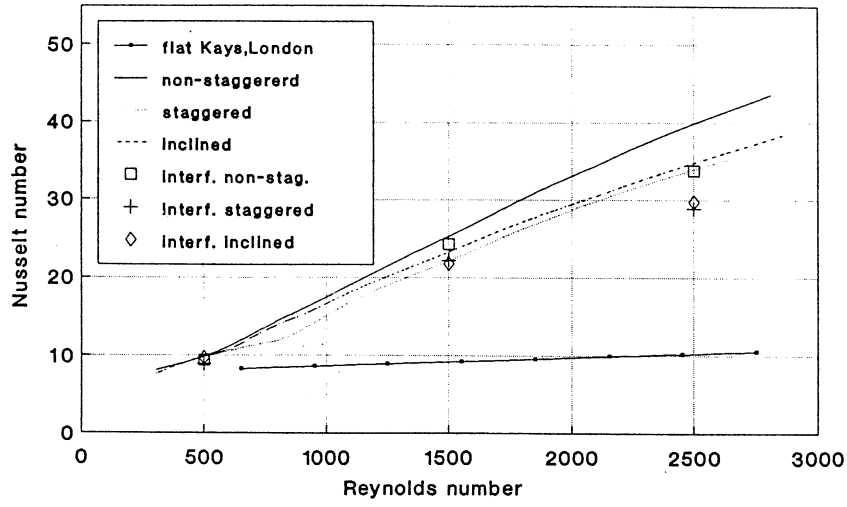

Figure 16. Nusselt number as a function of Reynolds number for circular segment shaped obstacles.

d_{hyd} hydraulic diameter, m
E fluid pumping power per unit surface area, W/m^2
e rib height, m
h heat transfer coefficient, W/(m^2 K)
$h_{\alpha,x}$ local heat transfer coefficient, W/(m^2 K)
k fluid thermal conductivity, W/(m^2 K)
l length of test matrix, m
l_r fin length, rib length, m
$\dot{m}$ mass transfer rate, kg/s
Nu average Nusselt number, dimensionless
$\overline{\text{Nu}}$ average Nusselt number, dimensionless
Nu_α local Nusselt number for plan fin arrangement, dimensionless
Nu_x local Nusselt number for turbulence promoters, dimensionless
$\text{Nu}_{y/a}$ local Nusselt number for square channel, dimensionless
p rib spacing, m
P pumping power, W
$\dot{q}_{\alpha,x}$ local heat flux density, W/m^2
$\dot{Q}$ heat transfer rate, W
Re Reynolds number ($= \rho w_m D_{hyd}/\mu$), dimensionless
T temperature, K
t_f fin thickness, m
ΔT_m logarithmic mean temperature difference, K
U overall conductance, W/(m^2 K)
V heat exchanger volume, m^3
w_m fluid mean axial velocity, m/s
x coordinate in flow direction, dimensionless
y coordinate perpendicular to the wall, dimensionless

Greek Symbols

α angle coordinate, dimensionless
β heat transfer surface area density, m^2/m^3
γ angle of attack, deg
μ fluid dynamic viscosity, Pa s
η_R fin efficiency, dimensionless
ν kinematic viscosity, m^2/s
φ circular segment angle, deg
ρ fluid density, kg/m^3
ξ pressure drop coefficient, dimensionless

This work is supported by the Federal Minister for Research and Technology of the Federal Republic of Germany through Forschungszentrum Jülich GmbH and assisted by the Motoren u. Turbinen-Union, München.

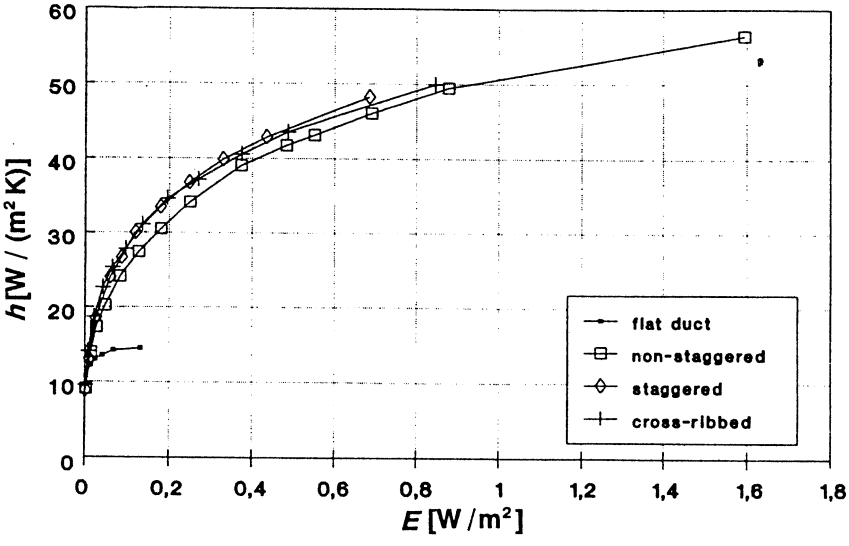

Figure 17. Volume goodness factor for different arrangements with turbulence promoters.

REFERENCES

[1] Shah, R.K., Compact and enhanced heat exchangers, in *Heat Exchangers - Theory and Practice*, J. Taborek, G.F. Hewitt and N. Afgan, McGraw-Hill Book Company, 1983.

[2] Shah, R.K., Classification of Heat exchangers, in *Heat Exchangers - Thermal Hydraulic Fundamentals and Design*, S. Kakac, A.E. Bergles and F. Mayinger, McGraw-Hill Book Company, 1981.

[3] Hauf, W., and Grigull, U., Optical Methods in Heat Transfer, in *Advances in Heat Transfer*, Vol. 6, pp. 133–366, Academic Press, New York, 1970.

[4] Chen, Y.M., and Mayinger, F., Holographic interferometry studies of the temperature field near a condensing bubble, in *Optical methods in the dynamics of fluids and solids*, M. Pachal, Proc. of an int. sympos, IUTAM, Berlin, Sept. 1985.

[5] Mayinger, F., and Panknin, W., Holography in heat and mass Transfer, Proc. of the 5th Int. Heat Transfer Conference, Tokio, Vol. VI, pp. 28–43, 1974.

[6] Marco, S.M., and Han, L.S., A Note on Limiting Laminar Nusselt Number in Ducts with Constant Temperature Gradient by Analogy to Thin Plate Theory, J. Heat Tranfer, Vol. 77, pp. 625–630, 1955.

[7] Luo, X., and Cai, Z.-H., Numerical Study of the Friction and Heat Transfer Performance of Straight Plate-Fin Surfaces, Int. Symp. on Heat Transfer, pp. 218–227, Peking, 1985.

[8] Kato, S., and Maruyama, N., Holographic Interferometry Measurements of the Three-Dimensional Temperature Field with Thermally Developing Flow in the Measuring Beam Direction, Proceedings of the 1st World Conference on Experimental Heat Transfer, Fluid Mechanics and Thermodynamics, pp. 425–431, Dubrovnik, 1988.

[9] Nikuradse, J., Untersuchungen über turbulente Strömungen in nicht kreisförmigen Rohren, Ingenieur Archiv, VDI 281, pp. 306–331, 1926.

[10] Prandtl, L., Über ausgebildete Turbulenz, 2. Int. Kongreß für Techn. Mechanik, Zürich, 1926.

[11] Brundrett, E., and Burroughs, P.R., The Temperature Inner-Law and Heat Transfer for Turbulent Air Flow in a Vertical Square Duct, Int. J. Heat Mass Transfer, Vol. 10, pp. 1133–1142, 1967.

[12] London, A.L., and Ferguson, C.K., The Results of High-Performance Heat Exchanger Surfaces Used in Aircraft Intercoolers and their Significance for Gas-Turbine Regenerators Design, J. Heat Transfer, Vol. 71, 1949.

[13] Kays, W.M., and London, A.L., The Gas-Turbine Regenerator – the Use of Compact Heat Transfer Surfaces, Trans. ASME, Vol. 72, 1949.

[14] Shah, R.K., and London, A.L., Laminar Flow Forced Convection in Ducts, Supplement 1 to Advances in Heat Transfer, Academic Press, New York, 1978.